# Terahertz band gap properties by using metal slits in tapered parallel-plate waveguides

Eui Su Lee, Young Bin Ji, and Tae-In Jeon[a)]
*Division of Electrical and Electronics Engineering, Center for Subwavelength Optics, Korea Maritime University, Busan 606-791, Republic of Korea*

(Received 15 September 2010; accepted 19 October 2010; published online 5 November 2010)

We present experimental and finite-difference time-domain simulation studies on the properties of Bragg and non-Bragg band gaps; the studies are carried out by using metal slit arrays positioned at the center of the air gaps in tapered parallel-plate waveguides. Two Bragg stop bands, with a dynamic power transmission range of about 26 dB, are observed for an air gap of 29 $\mu$m. Two non-Bragg stop bands are observed for an air gap of 94 $\mu$m. Using the Ey field distribution and Poynting vectors, we confirm that the Ey field leaking from the slit and the Ey field propagating from another input vanish because they are out of phase. The Bragg and non-Bragg stop bands determined in the simulations show excellent agreement with those observed experimentally. © *2010 American Institute of Physics*. [doi:10.1063/1.3514558]

Low-loss and single transverse electromagnetic mode propagation in the terahertz (THz) region in metallic parallel-plate waveguides (PPWGs) has been employed in studies on spectroscopy,[1,2] photonic waveguides,[3,4] and surface plasmon coupling.[5] In addition, studies on the effect of a longitudinal metallic structure such as a periodic array of grooves on the waveguide plate surfaces have been performed by using two-dimensional finite-difference time-domain (FDTD) simulations.[6,7] THz surface plasmon propagation on periodic plasmonic structures such as slits and rectangular apertures has also been experimentally studied.[8,9] The electromagnetic fields with the stop-band frequency are strongly localized on the grooves or slits, and therefore, they cannot be detected at the end of the periodic surfaces. Since the edges of the grooves or slits define a series of waveguide junctions, they are important in determining the characteristics of the band gaps.

Recently, researchers have investigated the use of a tapered parallel-plate waveguide (TPPWG)[10] and a smoothly curved metal flare waveguide[11] without a cylindrical silicon lens for improving THz coupling to the plate-separation air gap. The TPPWG has three advantages when forming Bragg stop bands using slits. The first is that (as mentioned above) it increases the intensity of THz fields in the air gap. The second is its ability to measure long scans without reflection. On the other hand, when the PPWG is used in long scans, problems arise because of reflection from the cylindrical silicon lens.[12] This is useful when dealing with chemical samples that require long scans to characterize molecular motion. The third advantage is that when dealing with slits that are located in the center of the air gap, the THz wave can propagate along the upper and lower surfaces of the sample because of the two tapered structures of the waveguide. In contrast, the cylindrical silicon lens used with the PPWG allows only one line-focus to the plate separation. In this paper, we use experimental measurements and FDTD simulations to investigate the Bragg and non-Bragg stop bands by positioning metal slits at the center of the air gap of the TPPWG.

The experimental setup is illustrated schematically in Fig. 1. The stainless steel slits have width w=60 $\mu$m, period p=150 $\mu$m, and thickness t=30 $\mu$m where the propagated THz beam width on the slits is d=5 mm. The slits are made by micro-photochemical etching (Youngjin Astech Co.).[8] The total number of slits is 15 and the total length of the stainless steel sheet is 20 mm. The slit surfaces are separated from the upper and lower plates of the waveguide, which maintain a constant air gap (g). We used two different air gaps, g=29 $\mu$m and g=94 $\mu$m, to study the properties of Bragg and non-Bragg band gaps. As shown in Fig. 1, the slits are installed on only one side. As the waveguide is moved a unit in the z direction, the reference and output THz pulses can be detected without any optical or mechanical adjustment. The angle of the tapered part is 3°; it has twice the coupling coefficient of the cylindrical silicon lens used in PPWG.[10] The total length of the flat surface of the TPPWG is k=6 mm. The protruded length of the stainless steel sheet in the tapered part is $\ell$=7 mm, and this can separate the incoming THz beam into two parts. Although the stainless steel sheet is located at the vertical center of the incoming THz beam, the measured spectrum has no distortion. This is because of the thin metal sheet and because the THz beam is not fully focused at the beginning of the protruded sheet. Since the polarization of the incoming THz beam is perpendicular (y-direction) to the slit surface, only TM modes exist.

Measurements of THz pulses with 29 and 94 $\mu$m air gaps are shown in Figs. 2(a) and 2(d). The inset in each figure shows the ringing structure caused by the slits. The measured pulse trains decay much faster than in Ref. 6 be-

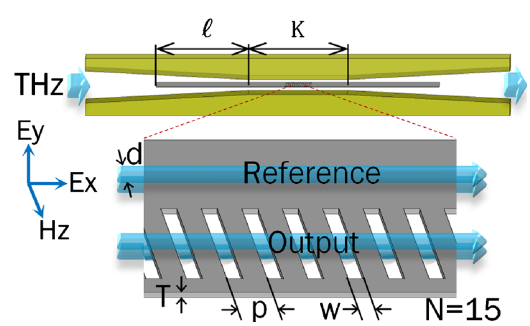


FIG. 1. (Color online) Diagram of TPPWG and slit sample.

a)Electronic mail: jeon@hhu.ac.kr.

 

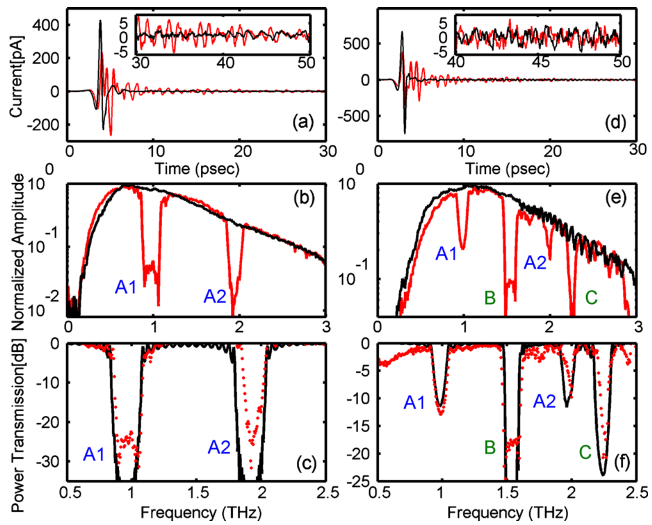


FIG. 2. (Color online) (a) Reference [black line (big pulse), without slits] and output [red line (small pulse), with slits] THz pulses for a 29 $\mu$m air gap. (b) Normalized amplitude spectra of the reference and output. (c) Comparison of power transmission spectrum between measurement (dots) and FDTD simulation (solid line). (d)–(f) are the same as (a)–(c) but for a 94 $\mu$m air gap.

cause the THz beam propagates through both the upper- and lower-side surfaces of the slits. Therefore, the measured pulse trains have been truncated to about 66 ps in the measurement. Because of a high order mode, the inserted reference signal of Fig. 2(d) shows a larger ringing signal than that seen in Fig. 2(a). The reference spectrum shown in Fig. 2(e) has oscillation from about 1.59 THz, which indicates the cutoff frequency of the $TM_1$ mode. The generated reference and output $TM_1$ modes by the upper and lower symmetric air gaps are coupled at the exit end of the stainless steel sheet. Therefore, the receiver can detect the coupled signals. The magnitude of the $TM_1$ mode has little effect on the result because of its small amplitude. Also, the output spectrum has the same $TM_1$ mode. Figures 2(b) and 2(e) show the spectra of each measured THz pulse. The upper black curves indicate the reference pulse spectrum without slits on the stainless steel sheet. Although the reference and output samples are one unit, there are system errors to the measured signals, especially the small air gap measurement. In addition, the attenuation of reference, which has two 29 $\mu$m air gaps, is bigger than that of the output, which has an 88 $\mu$m air gap between two waveguide plate surfaces (at the space of slit). Therefore, the reference amplitude is lower than the signal amplitude in some frequencies at the 29 $\mu$m air gap. Because of the periodic slit array, the Bragg stop bands are given by $f_{Bragg}=(m\cdot c)/(2\cdot p)$, where c is the speed of light and m is an integer. For a 150 $\mu$m slit period, the Bragg stop bands (A1 and A2 in the figures) occur at 1 and 2 THz for $m=1,2$ as shown in Figs. 2(b) and 2(e). Figure 2(e) shows not only the Bragg stop bands but also the non-Bragg stop bands (B and C in the figure). The stop bands are clearly observed from the power transmission as shown in Figs. 2(c) and 2(f). The dots and solid line indicate the experimental and FDTD simulation results, respectively, and the results are in good agreement. When the air gap is small, the electric field strongly couples between the waveguide plates and the slit surfaces. Therefore, the dynamic ranges of the Bragg band gap become strong (and form a stop band). When the air gap increases, the reflected THz beam from each slit becomes small and forms a weak band gap.[8] The dynamic range of the power transmission of the A1 Bragg stop band at the 94 $\mu$m air gap is reduced to approximately 12.5 dB as shown in Fig. 2(f). The dynamic range decreases with an increase in the air gap, which means that the THz beam propagated to the exits also increases. However, the dynamic ranges of the non-Bragg stop bands are stronger than those of the Bragg stop bands as shown in Fig. 2(f). To understand the properties of the Bragg and non-Bragg stop bands, we performed FDTD simulations.

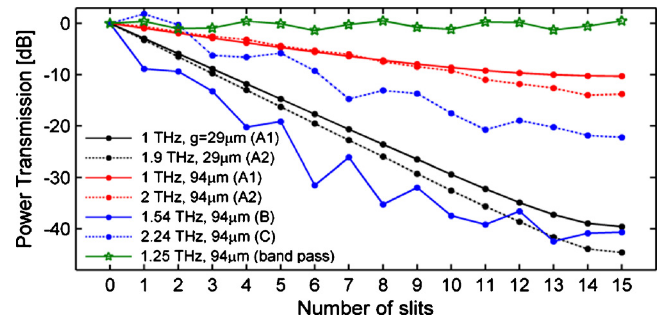


FIG. 3. (Color online) Comparison of power transmission for normalized time-averaged E field intensity according to the number of slits. The position of the measured average E field intensity is between slits (on the metal surface).

Figure 3 shows the comparison of power transmission for normalized time-averaged E field intensity variation along the position of slits. The amplitude of the Bragg stop bands (A1 and A2) at the 29 and 94 $\mu$m air gap and the non-Bragg stop bands (B and C) at the 94 $\mu$m air gap dramatically decrease with an increase in the number of slits. The E field intensity of the C stop band is enhanced after the first slit because of the merged reflection of the E field from higher-order slits such as the second and third slits. The amplitude of the A1 and A2 stop bands, at the 94 $\mu$m air gap, slowly decreases with an increase in the number of slits. Therefore, the E field intensity remains after 15 slits, which leads to the small dynamic range of the power transmission. The amplitude of the E field intensity, at 1.25 THz with a 94 $\mu$m air gap, has not attenuated with an increased number of slits, which shows the pass-band property.

The first and second measured central Bragg stop-band frequencies are 1 and 1.9 THz with $g=29$ $\mu$m. The intensity of the 1 THz E field dramatically decreases with propagation along the slits. The FDTD computation shows that the E field transmittance at the first slit is about 50%. After the input E field has propagated through 15 slits, only 0.01% of the E field intensity remains. Thus, the dynamic range of the power transmission is approximately 40 dB, which is larger than the experimental result (26 dB). However, both results are very small to be compared to the dynamic range of the nonstop-band frequency (pass band), for example 0.08 dB at 1.25 THz (29 $\mu$m air gap). Most of the Bragg reflections are performed in the initial section of the slits. The input THz E field intensity is only 27% (35%) after passing the second slit at 1 THz (1.9 THz). However, some of the E field propagates to the end of the slit for the measured central Bragg stop-band frequencies as 1 and 2 THz with $g=94$ $\mu$m. Because of the large air gaps, the E field transmittance is increased to about 80% (86%) after passing the first slit at 1 THz (2 THz). The dynamic range of the power transmission for 15 slits is 10.1 dB (8.6 dB) at 1 THz (2 THz). This is in good agree-

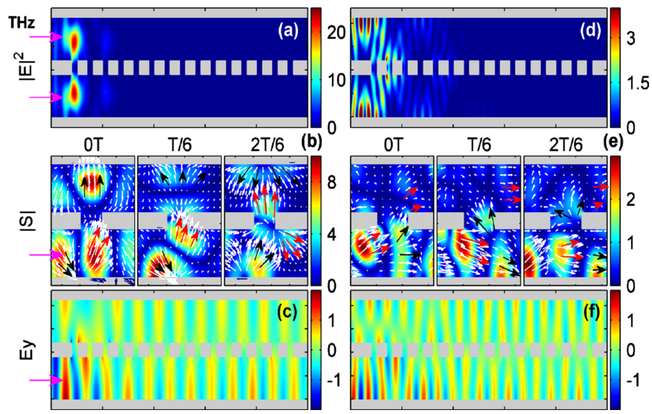


FIG. 4. (Color online) FDTD simulation with a 94 $\mu$m air gap. The left-hand figures illustrate the B stop-band frequency (1.54 THz), and the left arrowhead indicates THz beam entry to the air gaps: (a) E field intensity distribution; (b) Poynting vectors around the first slit (black and red arrows indicate $\pi$ radian phase difference); (c) Ey field distribution. The right-hand figures illustrate the C stop-band frequency (2.24 THz); (d) E field intensity distribution; (e) Poynting vectors around the third slit; (f) Ey field distribution.

ment with the experimental results: 12.5 dB (9.8 dB) at 1 THz (2 THz).

Figure 4(a) shows the E field intensity distribution of the B stop band at 1.54 THz and a 94 $\mu$m air gap. Most of the E field concentrates at the first slit. The FDTD computation shows that the E field transmittance is only 13.3% at the first slit. When the E field propagates to the first slit, some leaks into the slit gap. The leaked E field comes out from the opposite slit exit and radiates. Most of the radiated field is reflected from the surface to the opposite waveguide plate as shown in Fig. 4(b), which shows the poynting vector around the first slit. Figure 4(b) shows the situation after 108.2 fs time intervals, each corresponding to 1/6 of the time period of T which is 1/wavelength. Figure 4(c) shows the Ey field distribution. The polarities of the Ey field in the upper and lower air gaps are out of phase except at the front part of the slit. When the E field appears on both sides of air gap (upper and lower), the Ey fields that leak from the slit and propagate from the other input side are out of phase. Therefore, the two Ey fields vanish in the air gap. After the input E field has propagated through 15 slits, the dynamic range of the power transmission in the simulation is approximately 33 dB. As shown in Fig. 2(f), the measured dynamic range is about 19 dB. To compare the dynamic ranges, we set the pass band frequency to 1.25 THz. The dynamic range of the power transmission is only 0.12 dB at the pass band. Figures 4(d)–4(f) are as for Figs. 4(a)–4(c) but for the C stop band. Figure 4(e) shows the poynting vector around the third slit, illustrating the situation after 74.4 fs time intervals, each corresponding to 1/6 of the time period of T. This is the same mechanism seen for the B stop band, but now only a few front slits were needed to make the fields out of phase.

The air gap changes from 10 to 100 $\mu$m on the three-dimensional (3D) absorbance graph shown in Fig. 5. Because the Bragg stop bands (A1 and A2 in the figure) depend only on the period of the slits and not on the air gap variations, the stop bands always exist at 1 and 2 THz. The magnitude and width of the A1 and A2 stop bands are reduced and narrowed with an increase in the air gap. This is caused by weak coupling between the waveguide plates and the metal surface of the slit. Meanwhile, the non-Bragg stop

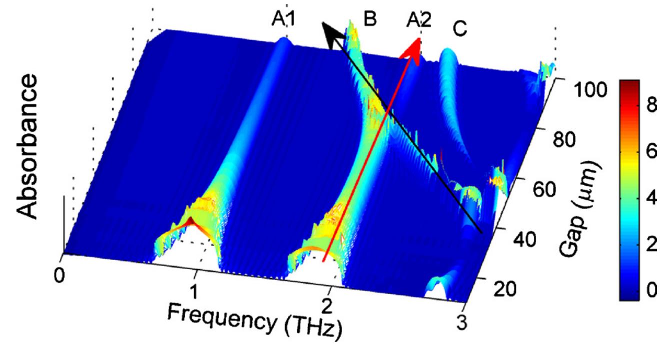


FIG. 5. (Color online) 3D THz absorbance graph for Bragg (A1 and A2) and non-Bragg (B and C) stop bands with different air gaps.

bands are caused by the wavelength/2 delay (out of phase) between the leaked Ey field by the slit and the propagated another Ey field. This means that the frequency of the non-Bragg stop band is in inverse proportion to the air gap and the smallest air gap exists around wavelength/2 of the measured maximum frequency. Therefore, the B and C stop bands are enhanced and shifted to lower frequencies with an increase in the air gap.

In summary, the Bragg stop bands depend only on the periodic slit intervals, whereas the non-Bragg stop bands depend on both the slit intervals and the air gap between the slit and the waveguide plate. The TPPWG was useful in the controlling the stop band because the THz beam propagates simultaneously through the upper- and lower-side air gaps. When the THz beam leaked through the slit and was reflected from the waveguide plate, the Ey field was out of phase relative to the Ey field of the incoming THz beam. Therefore, the two fields were coupled and vanished, giving rise to non-Bragg stop bands. By adjusting the air gap or the slit dimensions, we can control the non-Bragg stop bands. We simulated the Bragg and non-Bragg stop bands using FDTD simulation and found that they agreed well with the experimentally observed bands.

This work was supported by the Korea Science and Engineering Foundation (KOSEF) (SRC, Grant No. R11-2008-095-01000-0) and Basic Research Program through the National Research Foundation of Korea (NRF) funded by the Ministry of Education, Science and Technology (Grant No. 2010-0009070).

[1]J. Zhang and D. Grischkowsky, Opt. Lett. **29**, 1617 (2004).
[2]D. G. Cooke and P. U. Jepsen, Phys. Status Solidi A **206**, 997 (2009).
[3]Z. Jian, J. Pearce, and D. Mittleman, Semicond. Sci. Technol. **20**, S300 (2005).
[4]A. Bingham and D. Grischkowsky, IEEE Microw. Wirel. Compon. Lett. **18**, 428 (2008).
[5]M. Gong, T.-I. Jeon, and D. Grischkowsky, Opt. Express **17**, 17088 (2009).
[6]A. L. Bingham and D. Grischkowsky, Appl. Phys. Lett. **90**, 091105 (2007).
[7]K. Song and P. Mazumder, IEEE Trans. Microwave Theory Tech. **56**, 2792 (2009).
[8]E. S. Lee, D. H. Kang, A. I. Fernandez-Dominguez, F. J. Garcia-Vidal, L. Martin-Moreno, D. S. Kim, and T.-I. Jeon, Opt. Express **17**, 9212 (2009).
[9]A. K. Agrawal, H. Cao, and A. Nahata, Opt. Express **15**, 9022 (2007).
[10]S.-H. Kim, E. S. Lee, Y. B. Ji, and T.-I. Jeon, Opt. Express **18**, 1289 (2010).
[11]M. Theuer, R. Beigang, and D. Grischkowsky, Appl. Phys. Lett. **96**, 191110 (2010).
[12]N. Laman, S. S. Harsha, D. Grischkowsky, and J. S. Melinger, Opt. Express **16**, 4094 (2008).